Measurement of the thermal properties of unsaturated compacted soil by the transfer function estimation method

M. Lahoori, Y. Jannot, S. Rosin-Paumier, A. Boukelia, F. Masrouri

▶ **To cite this version:**

M. Lahoori, Y. Jannot, S. Rosin-Paumier, A. Boukelia, F. Masrouri. Measurement of the thermal properties of unsaturated compacted soil by the transfer function estimation method. Applied Thermal Engineering, 2020, 167, pp.114795. 10.1016/j.applthermaleng.2019.114795 . hal-02439493

HAL Id: hal-02439493
https://hal.science/hal-02439493v1

Submitted on 21 Jul 2022

HAL is a multi-disciplinary open access archive for the deposit and dissemination of scientific research documents, whether they are published or not. The documents may come from teaching and research institutions in France or abroad, or from public or private research centers.

L'archive ouverte pluridisciplinaire **HAL**, est destinée au dépôt et à la diffusion de documents scientifiques de niveau recherche, publiés ou non, émanant des établissements d'enseignement et de recherche français ou étrangers, des laboratoires publics ou privés.

Distributed under a Creative Commons Attribution - NonCommercial 4.0 International License

Version of Record: https://www.sciencedirect.com/science/article/pii/S1359431119332028
Manuscript_4e69e1a889a2f8051df1dbb5958d2330

Measurement of the thermal properties of unsaturated compacted soil by the transfer function estimation method

Lahoori, M. [a*], Jannot, Y. [a], Rosin-Paumier, S.[a], Boukelia, A. [a,b], Masrouri, F.[a]

a LEMTA – CNRS UMR 7563, Université de Lorraine, Vandoeuvre-lès-Nancy, F-54500, France.

b ESITC de Metz, Metz, France

Current email addresses of authors:

mojdeh.lahoori@univ-lorraine.fr

yves.jannot@univ-lorraine.fr

sandrine.rosin@univ-lorraine.fr

Boukelia.a@gmail.com

farimah.masrouri@univ-lorraine.fr

*Corresponding author:

mojdeh.lahoori@univ-lorraine.fr

sandrine.rosin@univ-lorraine.fr

Postal address: ESNG - LEMTA, Bâtiment E, 2 rue du Doyen Marcel Roubault, TSA 70605, 54518 Vandoeuvre-lès-Nancy, France

© 2019 published by Elsevier. This manuscript is made available under the CC BY NC user license
https://creativecommons.org/licenses/by-nc/4.0/

Abstract:

Thermal energy storage in embankments can be considered a new economically efficient and environmentally friendly technology in geotechnical engineering. In these structures, horizontal heat exchanger loops can be installed inside different layers of compacted soil to store heat in the medium during the summer to be extracted during the winter. Compacted soils are usually unsaturated; therefore, reliable estimates and measurements of unsaturated compacted soil thermal properties, such as the volumetric heat capacity, thermal conductivity, and thermal diffusivity, are important in the efficiency analysis of these structures. However, there is no available method to characterize the evolution of these parameters over time in compacted soil.

In this study, several temperature sensors were placed inside different layers of unsaturated compacted soil in a cylindrical container (height of 0.8 m and diameter of 0.6 m) to monitor imposed temperature cycle variations. An inverse analytical model based on the one-dimensional radial heat conduction equation is proposed to estimate the thermal diffusivity using the temperature variation between two temperature sensors. The volumetric heat capacity was measured with a calorimeter in the laboratory, enabling estimation of the thermal conductivity of the compacted soil. Then, this estimated thermal conductivity was compared with the thermal conductivity values measured with two different methods (one steady-state and one transient-state method). The estimated thermal conductivity was close to the value measured with the transient-state method. It was demonstrated that steady-state methods are not suitable for the measurement of thermal conductivities as high as 2.5 $\mathrm{W.m^{-1}.K^{-1}}$ since thermal contact resistances are no longer negligible.

Keywords: Soil thermal properties, transfer function, unsaturated compacted soil, inverse analytical model

1 Introduction

In recent years, due to the depletion of fossil resources and their negative impact on the environment, there is a tendency towards using renewable energy. Among the different types of renewable energies, solar energy provides an abundant, clean and safe energy source. The supply of this energy is periodic, following yearly and daily cycles [1]. Various techniques have been developed to store solar energy in a proper medium for use in high-demand periods. Thermal energy storage is a technique that can be described as the short- or long-term storage of thermal energy by heating a storage medium. Seasonal thermal energy storage stores solar energy that is diffused in the summer for space heating in the winter [2]. Thermal energy can be stored by inserting vertical or horizontal heat exchanger loops into a storage medium. Several studies have shown that seasonal thermal energy storage is a pertinent technique that has been used in geologic storage media, such as soil, due to its appropriate thermal properties and ease of access [3,4].

In geotechnical engineering, different types of structures are made of unsaturated compacted soil, for example, road and rail embankments and dikes. Generally, these linear structures contain several layers of unsaturated compacted soils. Horizontal heat exchanger loops can easily be installed in these layers during the construction phase (Figure 1) [5,6].

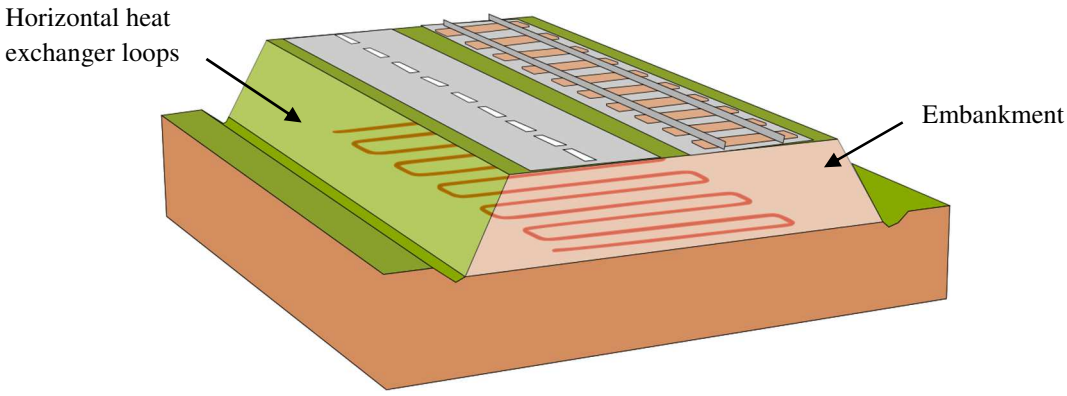

Figure 1: Forecast embankment thermal storage.

However, the cyclic temperature variations in these structures could modify the thermo-hydro-mechanical (THM) behaviour of the soil, and these variations may consequently affect the expected mechanical performance of the structures and heat storage efficiency [7,8,9]. Therefore, a more comprehensive understanding of the following aspects is needed:

1) Determination of the thermal characteristics of unsaturated compacted soil to optimize the heat storage energy amount.

2) Examination of the effect of temperature variations on the THM behaviour of unsaturated compacted soil.
3) Investigation of the interaction between unsaturated compacted soil and heat exchanger loops.

This study focuses on the thermal parameters of unsaturated compacted soil to optimize the efficiency of thermal storage structures. The thermal properties that affect the heat storage capacity are the volumetric heat capacity C_v ($J.m^{-3}.K^{-1}$), the thermal conductivity λ ($W.m^{-1}.K^{-1}$) and the thermal diffusivity α ($m^2.s^{-1}$). The relationship between these thermal properties is as follows:

$$\alpha = \frac{\lambda}{C_v} \quad (1)$$

The soil thermal properties change according to its physical and hydro-mechanical properties, such as the mineral composition, degree of saturation and dry density [10-12]. The variation of these properties coupled with the thermal solicitations in unsaturated soil can reach a high level of complexity, which causes difficulties in evaluating the thermal properties of these soils [13]. Additionally, in an unsaturated medium, due to such a complex multiphase medium, heat is transferred by three different modes: conduction through the solid particles, convection through the gaseous and liquid phases, and radiation at the particle surfaces. However, due to the complex combination of these phases in unsaturated soil, most of the measurement and estimation methods applied to unsaturated soil to measure its thermal properties are based on the solution of a one-dimensional heat conduction equation assuming a homogeneous soil [14-16].

The thermal properties of soils can be measured indirectly with steady-state or transient-state methods by measuring the rise or fall of the temperature in response to a heat flux [17,18]. Steady-state methods are used to measure thermal properties when the heat transfer flux through the sample remains unchanged over time. The reference steady-state method to measure the thermal conductivity is the guarded hot plate method, which is performed on samples with a minimum cross-section of 0.3 x 0.3 m^2 [19,20]. The centred hot plate method enables measurement of the thermal conductivity of smaller samples, with a 0.1 x 0.1 m^2 cross-section [21,22].

Transient methods are used to measure thermal properties during the unsteady-state heat transfer process. The thermal needle probe and infrared thermal imaging methods are often used to measure the thermal conductivity and thermal diffusivity of soil samples in the laboratory

and field, respectively [14,19,23,24]. However, these transient methods only obtain a single reading at the corresponding time and cannot measure the temperature profile along the soil depth in the field, which is the inherent limitation of these techniques [15].

In the field, the thermal diffusivity can also be estimated by monitoring the temperature of the soil via a thermal response test [25, 26]. The thermal response test is commonly used to estimate the thermal properties of saturated soils based on the inlet and outlet temperatures of vertical heat exchanger loops, which are inserted several tens of metres into the ground [27,28].

The temperature monitoring method, using different temperature sensors at different depths, has been proposed to estimate the thermal diffusivity of unsaturated soils near the ground surface [15,29,30]. Based on these methods, different analytical and numerical models were proposed to predict the heat transfer function and consequently the apparent thermal diffusivity of the medium from the observed temperature variations.

Gao et al. [31] and Rajeev & Kodikara [15] used simplified analytical models under the hypothesis of a sinusoidal temperature variation in the soil surface (sinusoidal boundary condition), which is not always valid in thermal energy storage since the duration of the cooling period is not necessarily as long as the heating period. This type of temperature monitoring method was also used by Ukrainczyk [16] to estimate the thermal diffusivity of complex materials. In their study, a numerical inverse solution for one-dimensional heat conduction was used, which is more complex than the direct analytical model and was only used in the laboratory.

Jannot & Degiovanni [32] proposed a simple inverse analytical model to estimate the thermal properties of powders or granular materials. In this method, the transfer function is not dependent on the shape and intensity of the heat flux or the external boundary condition (such as the soil surface in the field). In this temperature/temperature method, first, the transfer function between two recorded temperatures is modelled, and then an associated inverse analytical model is proposed to estimate the thermal diffusivity. To our knowledge, this analytical model has never been applied to unsaturated compacted soils. In this study, this analytical model is adapted and applied to estimate the thermal diffusivity (α) of unsaturated compacted soil by monitoring the temperature of a large-scale sample when subjected to temperature variation cycles. Then, the volumetric heat capacity, C_v, was measured in the laboratory to estimate the thermal conductivity λ using Eq. (1). The estimated thermal conductivity was then compared with the thermal conductivities that were measured in the

laboratory via two other classical methods (the transient-state and steady-state methods). If the estimated thermal conductivity validated, this method could enable system efficiency estimation of possible future applications of thermal energy storage in compacted soils such as embankments or other configurations.

2 Materials and methods

In this section, the properties of the studied material are first presented, and then the different methods used to estimate the thermal properties of unsaturated compacted soil are detailed.

2.1 Material properties

The tested soil was extracted from the Paris region in France. X-ray diffractogram analysis revealed that the soil contains 81% quartz, 7% dolomite, 5% calcite, 5% clay minerals and 3% feldspar [33]. This material was dried, pulverized and passed through a 2 mm sieve before being used for the various experiments. According to the particle-size distribution, almost 20% of the soil particles were smaller than 2 µm, and 41% were smaller than 80 µm (Figure 2a). With a liquid limit (LL) of 27% and a plastic limit (PL) of 21%, the plasticity index (PI) was 6% [34]. The standard Proctor curve of the material [35] showed an optimum water content (w_{opt}) of 16% and a maximum dry density (ρ_d) of 1.81 $Mg.m^{-3}$ (Figure 2b).

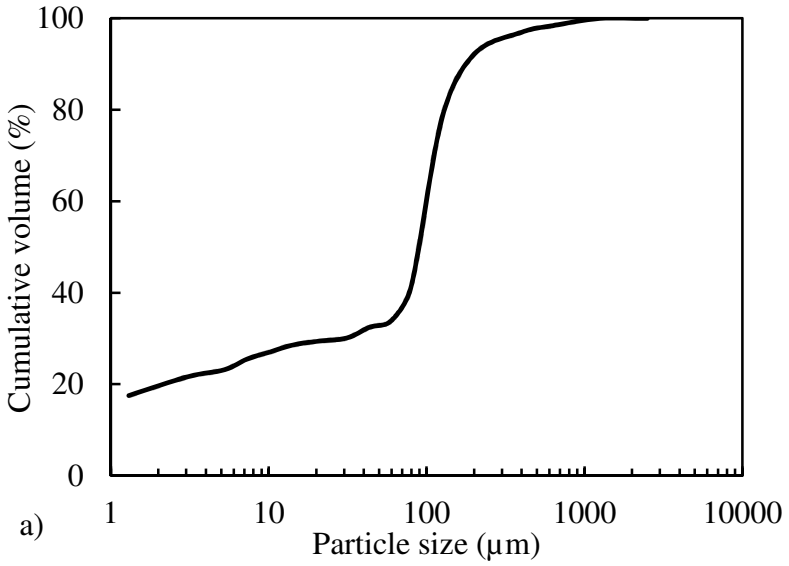

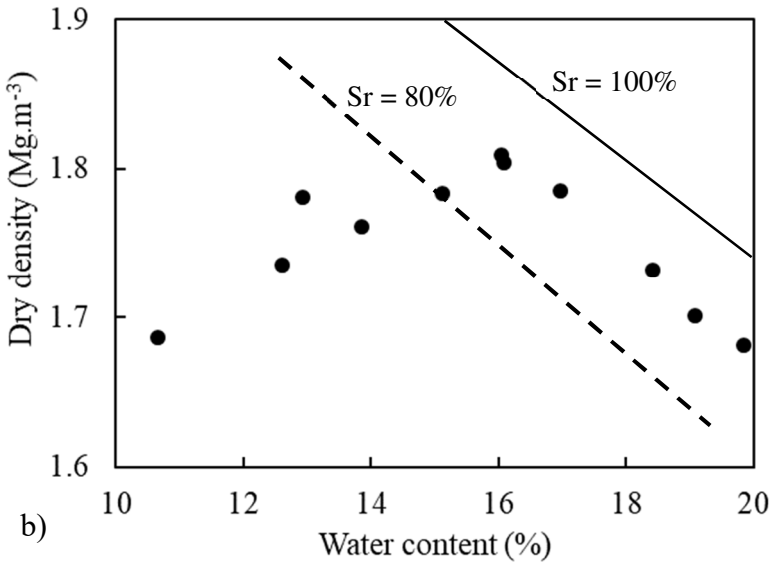

Figure 2: Characteristics of the studied soil: a) particle size distribution and b) compaction curve, Sr: The degree of saturation.

The material was classified as a sandy lean clay, CL, according to the Unified Soil Classification System [36] and as A1 in the French standard for soil classification [37].

To optimize the efficiency of thermal embankment storage, the variation of the thermal properties of the soil with the dry density and degree of saturation were investigated. In accordance with the literature, Bristow [38] and Smits et al. [39] observed that thermal properties increased with an increase in the degree of saturation or dry density. Boukelia et al. [33] showed that the maximum values of the thermal conductivity and volumetric heat capacity of the studied soil were reached at a water content of 16.3% and a dry density of 1.79 $\mathrm{Mg.\,m^{-3}}$. However, this compaction state could not be reached in the large-scale experimental container. As a consequence, the reference compaction state in this study was a water content of 16.3% and a dry density of 1.72 $\mathrm{Mg.\,m^{-3}}$.

2.2 Transfer function estimation method (TFEM)

To prepare the sample for temperature monitoring, the soil was compacted in a container with a height of 0.8 m and a diameter of 0.6 m with a pneumatic compactor (Figure 3a). This large-scale sample was realized to reproduce the in situ conditions. The compactor applied dynamic forces on a metallic plate, which was 0.04 m thick and 0.6 m in diameter, placed on top of the material to ensure homogeneous soil compaction. To ensure a homogeneous density the massif, compaction was performed in eleven 0.07 m thick layers.

Five temperature sensors, PT100 (6 mm in diameter and 60 mm in length), were positioned in

182 different layers of the compacted soil (T3 to T7, Figure 3a) and plugged into a data logger to
183 monitor the temperature variations inside the compacted soil. The temperature was recorded
184 every 50 s using the five temperature sensors. To induce cyclic variations of the temperature,
185 an ethylene glycol-water solution was circulated through a stainless steel tube which was
186 welded to the outside of the container (Figure 3c). A heating-cooling system (Vulcatherm
187 thermoregulator, with a 6 kW heating capacity) imposed three successive heating-cooling
188 cycles in the range of 20 to 50 °C (Figure 3d). Thermal equilibrium was reached for each step
189 before changing, and the entire test lasted one week. Insulating sleeves were placed around the
190 tube to reduce the amount of heat exchange with the surrounding atmosphere. Plastic film was
191 placed on top of the container to preserve the initial water content. Finally, the entire device
192 was placed in a box made of 0.04 m thick extruded polystyrene plates to reinforce the thermal
193 insulation effect (Figure 3c).

194 2.3 Water content and density profile measurements

195 Six cores with a diameter of 28 mm were positioned on a concentric circle with a diameter half
196 the size of that of the container (Figure 3b). The 630-mm-length cores were divided into small
197 segments to measure the water content and density of the material as a function of depth. The
198 measurements for two of the cores were conducted at the beginning of the test (20 a-b), and the
199 measurements for two other cores were carried out at the end of the first heating cycle (50 a-b),
200 while the two remaining cores were analysed at the end of the test (20 c-d) (Figure 3b, 3d).
201 These results allowed us to assess the initial homogeneity of the sample and to evaluate any
202 variations due to the temperature changes.

203

204

205

206

207

208

209

210

211

212

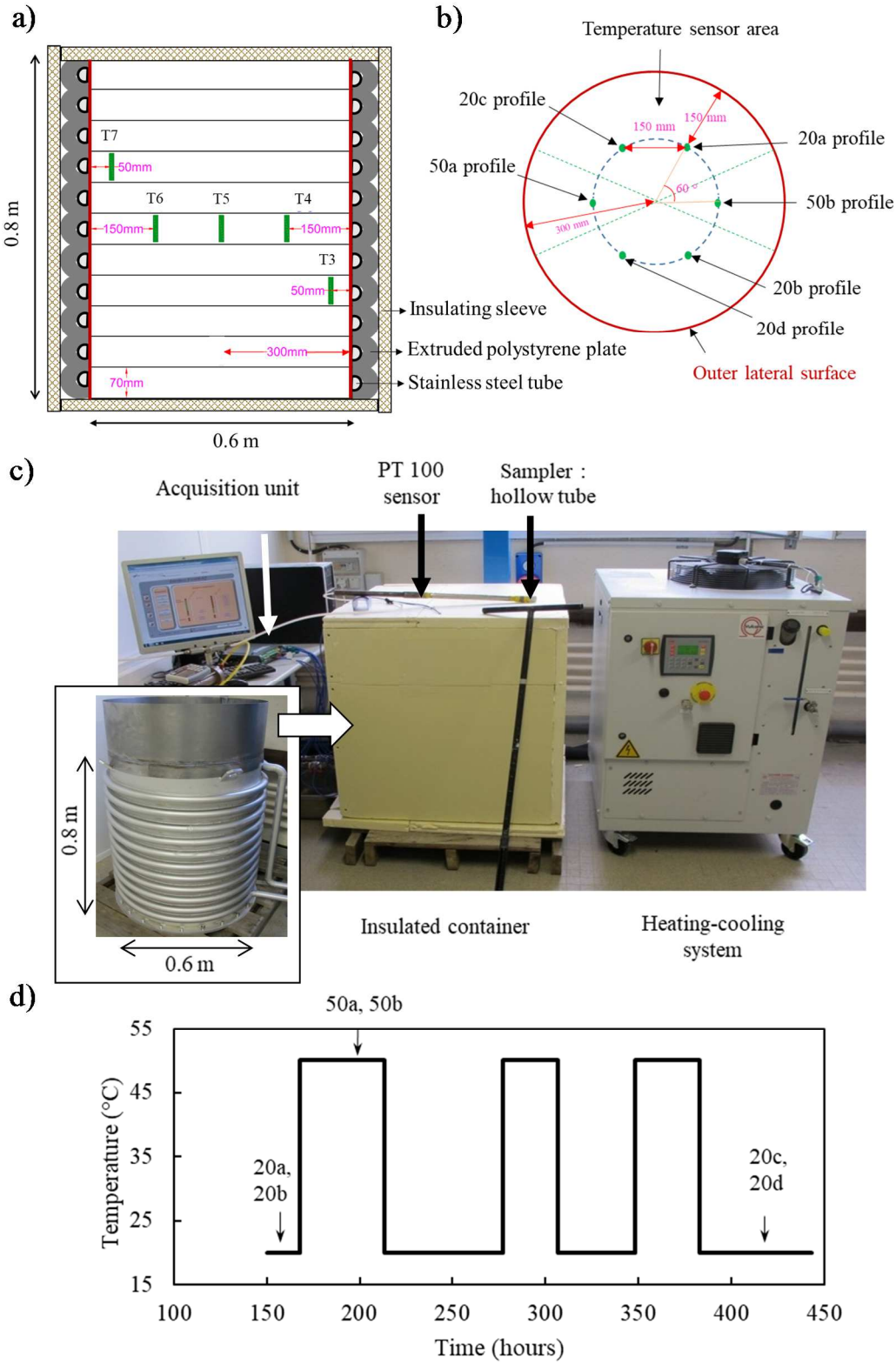

213

214 *Figure 3: Details of the developed laboratory model a) cross sectional view of the thermo-*
215 *regulated metric scale container and the place of the temperature sensors (T3 to T7) b) top*
216 *view of the thermo-regulated metric scale container and the position of the cores profiles: 20*
217 *a-b: two cores before first heating, 50 a-b: two cores after the first heating and 20 c-d: two*
218 *cores after the third heating and cooling cycle c) experimental setup d) three temperature cycles*
219 *imposed using heating and cooling system and cores section times.*

220 2.4 Other methods for measuring the thermal properties

221 To validate the proposed TFEM method, the thermal properties were measured by other
222 methods.

223 A micro-differential scanning calorimeter (DSC, SETARAM μdsc3) was used to measure the
224 specific heat (C_{dry}) of dry soil at different temperatures.

225 The specific heat (C_p) of soil at a certain mass water content (w) can be deduced by:

226 $$C_p = \frac{C_{dry} + w\, C_{water}}{1 + w} \quad (2)$$

227 where C_{water} is the specific heat of pure water (C_{water} = 4180 $J.kg^{-1}.K^{-1}$ at 20 °C).

228 The volumetric heat capacity C_v ($J.m^{-3}.K^{-1}$) is then given by:

229 $$C_v = \rho\, C_p \quad (3)$$

230 where ρ is the density of wet soil ($kg.m^{-3}$).

231 The thermal conductivity was also measured by two other methods:

232 - Transient-state method: a KD2 Pro Analyser and a single-needle probe (TR-1) with a 2.4
233 mm diameter and 100 mm length were used to measure the thermal conductivity of the
234 compacted soil samples. This method is a transient-state technique that measures the thermal
235 conductivity through the transient line heat source method [40]. The single-needle probe
236 (TR-1) was covered with a thin layer of grease to improve the contact between the probe and
237 the soil. Then, it was inserted into the sample that was already compacted in three layers at
238 the desired water content and dry density in a standard Proctor mould with a 0.116 m height
239 and 0.101 m diameter. A waiting time of 15 min was allowed before each test so that the
240 equilibrium temperature between the probe and the soil was reached. The presented values
241 are the mean values of 4 tests performed at different locations in the sample. The thermal
242 conductivity measurement range of this probe is from 0.2 to 4 $W.m^{-1}.K^{-1}$ with an accuracy
243 of ±10% [40].
244 - Steady-state method: the centred hot plate method [21,22] is a steady-state method that
245 consists of inserting a thin planar heating element between the soil and a reference material
246 of known thermal conductivity (Figure 4). A constant heat flux is produced by the heating
247 element. The soil samples were compacted in a special mould (0.1 x 0.1 x 0.02 m^3) via the
248 static compaction method (Figure 5a and 5b). The assembly was inserted between two
249 aluminium plates that were maintained at a constant temperature (T_0=15 °C) and placed in a
250 climatic chamber (Ta= 23 °C) (Figure 5c).

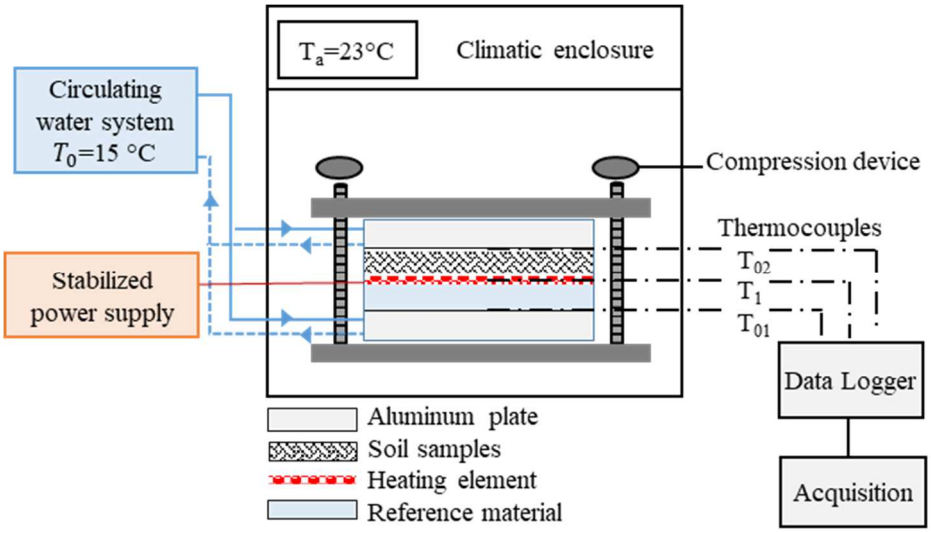

Figure 4: Scheme of hot plate device; where $\boldsymbol{T_1}$ is the temperature of heating element, $\boldsymbol{T_{01}}$ and $\boldsymbol{T_{02}}$ are temperatures of the aluminum plates and $\boldsymbol{T_a}$ is the temperature of the air.

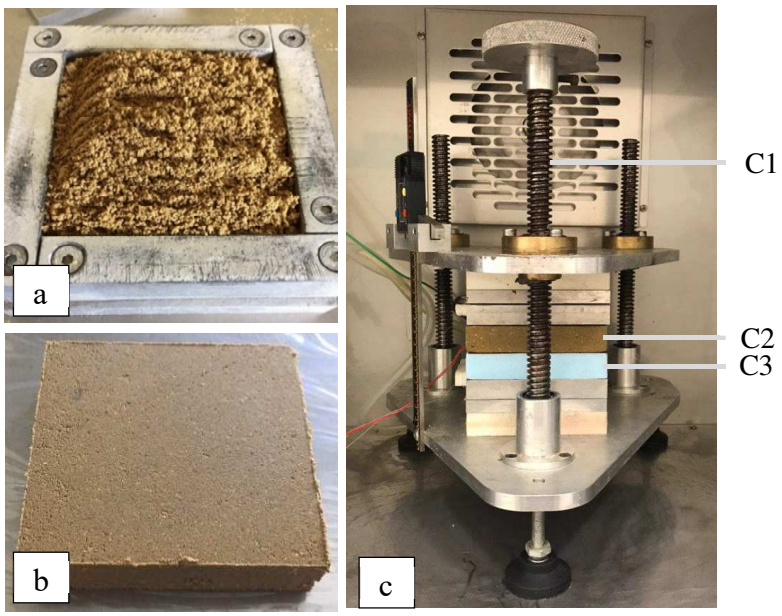

Figure 5: a) mold of sample preparation for centred hot plate tests b) compacted soil sample for centred hot plate test c) test assembly C1) Manually Compressing screw (Tightening device) C2) soil sample C3) reference material.

3 Modelling

3.1 The TFEM method

In this part, the inverse analytical model based on the one-dimensional solution of the Fourier heat balance equation is used to estimate the thermal diffusivity of the compacted soil based on the temperature variations between two temperature sensors.

The estimate of thermal diffusivity α ($m^2.s^{-1}$) is based on the estimation of the transfer function between the inlet and outlet temperatures inside the cylindrical sample. In this study, the heat flux is applied to the external surface of the cylindrical sample and as mentioned in the introduction, the transfer function is not dependent on the shape and intensity of the heat flux or the external boundary condition [32]. The following hypotheses are considered in this model:

- The initial temperature of the compacted soil inside the container is uniform;
- The heat transfer is 1D; and
- Mass transfer is neglected.

The inverse method is expressed by the following equations. The transient heat conduction in the radial direction in cylindrical coordinates is:

$$\frac{\partial^2 T}{\partial r^2} + \frac{1}{r}\frac{\partial T}{\partial r} = \frac{1}{\alpha}\frac{\partial T}{\partial t} \tag{4}$$

With the following boundary conditions:

$$\begin{cases} T(r, t = 0) = T_i,\ 0 \le r \le R & (5) \\ T(R, t) = T_0(t) & (6) \end{cases}$$

where T is the temperature (K), r is the radius (m) (the distance of the temperature sensors from the axis of the container), α is the thermal diffusivity ($m^2.s^{-1}$), t is the time (s), R is the radius of the container (m) and T_i is the initial temperature of the sample (K).

The following applies:

$$\overline{T} = T - T_i, \tag{7}$$

The Laplace transform of Eq. (4) results in Eq. (8), where p is the Laplace parameter (s^{-1}), $\theta(r, p)$ is the Laplace transform of $\overline{T}(t)$ and α is the thermal diffusivity ($m^2.s^{-1}$):

$$\frac{\partial^2 \theta}{\partial r^2} + \frac{1}{r}\frac{\partial \theta}{\partial r} = \frac{p}{\alpha}\theta \tag{8}$$

This equation may also be written as:

$$\frac{\partial^2\theta}{\partial u^2} + \frac{1}{u}\frac{\partial\theta}{\partial u} = \theta \qquad \text{with: } u = \sqrt{\frac{p}{\alpha}}r = qr \tag{9}$$

The general solution of this equation is [41]:

$$\theta(r,p) = AI_0(qr) + BK_0(qr) \tag{10}$$

where I_0 is the modified Bessel function of the first kind of order 0, K_0 is the modified Bessel function of the second kind of order 0, and A and B are constants.

The heat flux is null for $r = 0$ so $B = 0$ since $\lim_{r\to 0} K_0(qr) = 0$.

Hence: $$\theta(r,p) = AI_0(qr) \tag{11}$$

The Laplace transform H_p of the transfer function $F(t, \alpha)$ (s^{-1}) between the two temperatures $\overline{T}(r_2)$ and $\overline{T}(r_1)$ with $r_2 > r_1$ is:

$$H_p = \frac{\theta(r_2,p)}{\theta(r_1,p)} = \frac{I_0(qr_2)}{I_0(qr_1)} \tag{12}$$

This function only depends on the thermal diffusivity.

$$\theta(r_1,p) = \frac{I_0(qr_1)}{I_0(qr_2)}\theta(r_2,p) \tag{13}$$

$$\overline{T}(r_1,t) = \mathcal{L}^{-1}\left[\frac{I_0(qr_1)}{I_0(qr_2)}\right] \otimes \overline{T}(r_2,t) \tag{14}$$

where $\otimes$ is the convolution operator.

The thermal diffusivity α is estimated by minimizing the sum of the squared differences between the experimental curve $\overline{T}(r_1)$ and the modelled curve calculated by the relationship of the following type:

$$\overline{T}r_{1_{model}} = \overline{T}r_{2_{experimental}} \otimes F(t,\alpha) \text{ with: } F(t,\alpha) = \mathcal{L}^{-1}[H(p,\alpha)] \tag{15}$$

Minimization of the sum of the squared deviations is carried out with the Levenberg-Marquart algorithm, and the function $F(t,\alpha)$ is calculated with the inverse Laplace transform of Eq. (12) and the De Hoog algorithm [42]. As indicated in Eqs. (14) and (15), this analytical model depends on the thermal diffusivity and the transient temperature variations at distances r_1 and r_2 from the axis of the cylindrical sample. The temperature variations at different distances from the centre of the container were obtained from the experiments carried out in the laboratory.

3.2 Single-needle probe method

In this method, a heat flux is applied from a single stainless steel needle probe for a period of time, t_h (approximately 30 s), and then the cooling phase starts when the heat flux is stopped. For both the heating and cooling phases, the temperature variations are monitored every second. These temperature variations are then fit to the equations below [40].

The temperature during the heating phase:

$$T_h = m_0 + m_2 t + m_3 \ln t \quad (16)$$

The temperature during the cooling phase

$$T_c = m_1 + m_2 t + m_3 \ln \left[\frac{t}{t - t_h}\right] \quad (17)$$

where T is the temperature (K), t is the time, m_0 and m_1 are the ambient temperatures of the heating and cooling phases (K), respectively, m_2 is the rate of the background temperature drift ($K.s^{-1}$), and m_3 is the slope of the line relating the temperature rise to the logarithm of the temperature (K). Since Eqs. (16) and (17) are log time approximations, only the final 2/3 of the data collected are used for fitting, and the early time data are neglected during the heating and cooling phases [38]. Finally, the thermal conductivity is calculated using the following equation:

$$\lambda = \frac{Q}{4\pi m_3} \quad (18)$$

where λ is the thermal conductivity ($W.m^{-1}.K^{-1}$) and Q is the applied heat input rate per unit length ($W.m^{-1}$).

3.3 The centred hot plate method

The heat flux φ (W) produced in the heating element can be written as:

$$\varphi = \frac{\lambda_{ref}}{e_{ref}} (T_1 - T_{01}) + \frac{T_1 - T_{02}}{R_s} \quad (19)$$

where λ_{ref} and e_{ref} are the thermal conductivity ($W.m^{-1}.K^{-1}$) and thickness (m), respectively, of the reference material, T_1 is the temperature of the heating element (K), T_{01} and T_{02} are the temperatures of the aluminium plates (K) and R_s is the global thermal resistance ($K.m^2.W^{-1}$).

The global thermal resistance (sample and contact resistance) is given by:

$$R_s = \frac{T_1 - T_{02}}{\varphi - \frac{\lambda_{ref}}{e_{ref}} (T_1 - T_{01})} \quad (20)$$

337 and $R_s = \frac{e_s}{\lambda_s} + R_{c1} + R_{c2}$ (21)

338 where R_{c1} and R_{c2} are the thermal contact resistances on each side of the sample ($K.m^2.W^{-1}$).

339 The thermal conductivity may be calculated as follows:

340 $\lambda_s = \frac{e_s}{R_s - R_{c1} - R_{c2}}$ (22)

341 Neglecting these thermal contact resistances, one can deduce the following:

342 $\lambda_s = \frac{e_s}{R_s}$ (23)

343 where λ_s is the soil thermal conductivity ($W.m^{-1}.K^{-1}$) and e_s is the thickness of the soil
344 sample (m).

345 ## 4 Results and discussion

346 In the following, the homogeneity of the compacted soil is first verified, and then, the
347 temperature monitoring data inside the compacted soil and the inverse analytical model were
348 used to estimate the thermal diffusivity. Thereafter, the volumetric heat capacity of the material
349 was measured via the micro-calorimeter test to estimate the thermal conductivity of the
350 compacted soil.

351 ### 4.1 Water content and density profiles

352 The water content (w) and dry density (ρ_d) of the compacted soil were measured as a function
353 of the depth (from 200 to 580 mm depth) in six cores (Figure 6). At the initial state (20a-b), the
354 mean water content was 16.3%, and the mean dry density was 1.72 $Mg.m^{-3}$.

355 The water content was measured before starting the thermal cycles (20a-b), and the values were
356 close to the initial water content (16.3%) (Figure 6a). After the first heating cycle, there is a
357 water content gradient in terms of the radius of the cylindrical samples, and the water content
358 at the wall of the cylindrical sample near the heat flux decreased, while the water content at the
359 centre of cylindrical sample increased (50a-b). Consequently, the water content measurement
360 at a radius of R/2 (R is the radius of the container) is slightly lower than the initial water content
361 (-0.41%). At the end of the cycles, after the temperature has stabilized (20c-d Figure 3), the
362 water gradient has dissipated, and the water content at a radius of R/2 becomes equal to the
363 initial value of 16.3%.

364

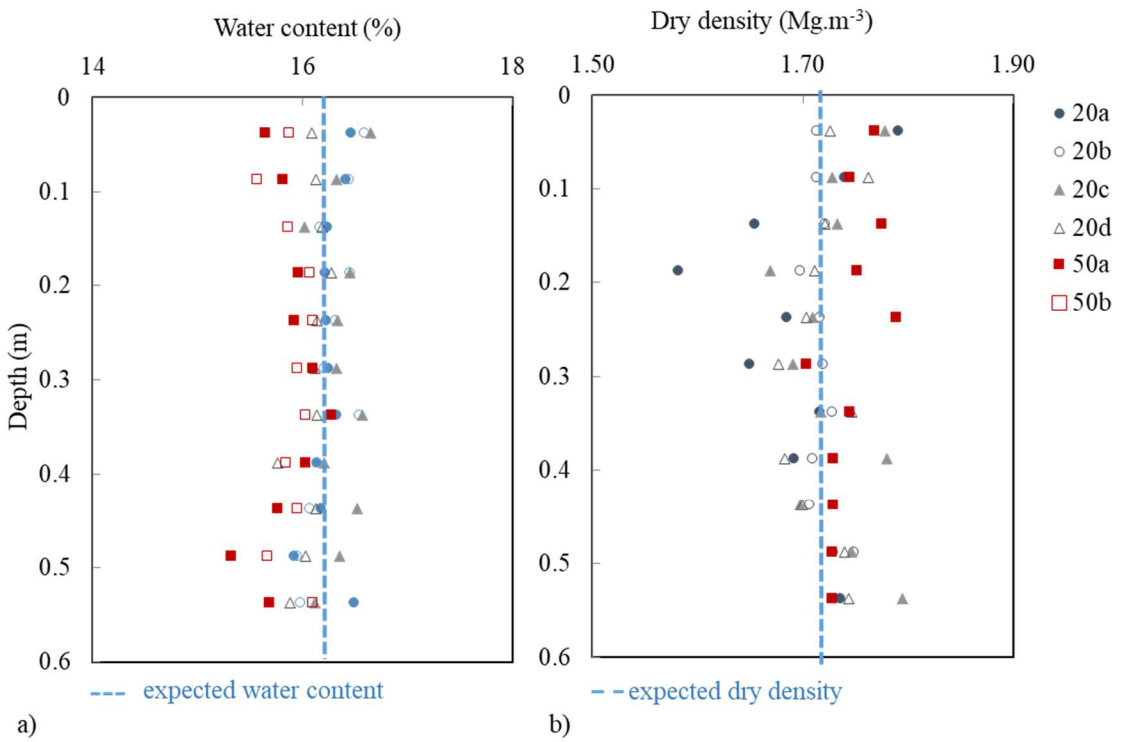

Figure 6: (a) water content profiles (b) dry density profiles along the depth of the container.

4.2 Sensitivity analysis of *the TFEM method*

The initial temperature of the compacted soil was 20 °C, and the soil was subjected to three heating cycles to 50 °C. The temperature variations were imposed through the outer lateral surface of the container, and the temperature variations were recorded by the different temperature sensors at the different positions in the container (see section 2.2 and Figure 3a for further details). Figure 7 shows the temperature records of the temperature sensors T3, T4, T5, T6, and T7. The time to reach equilibrium is different according to the distance between the temperature sensor and the source of the heat flux. Thus, temperature sensors T7 and T3, which were closer to the source, reached equilibrium quicker than the other temperature sensors that were further away.

As mentioned in the previous section (3.1), the analytical model was based on the temperature, the time, the thermal diffusivity and the distance from the centre of the container. First, the uniqueness of the solution was verified, and then the standard deviation and the errors due to the temperature and distance variations from the axis of the container were calculated.

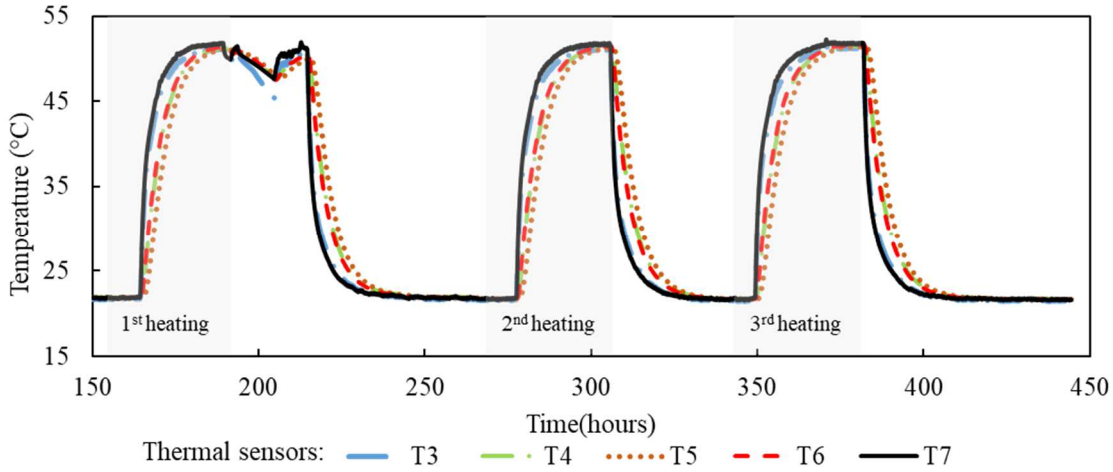

Figure 7 : Temperature variations in the compacted soil at various locations in the container: three heating-cooling cycles (20-50-20 °C).

4.2.1 Influence of the initial value of the thermal diffusivity

To verify the uniqueness of the solution, the analytical model was applied with several initial thermal diffusivities. In Eq. (15), the temperature variations recorded by the T6 sensor were used as Tr_2 and the T5 values as Tr_1. The analytical model has been applied with different initial thermal diffusivities (α) of 5.10^{-7}, 8.10^{-7} and 10.10^{-7} $m^2.s^{-1}$. For each test, the thermal diffusivity converges towards the same value, namely, $8.6.10^{-7}$ $m^2.s^{-1}$. The results showed that the value of the estimated thermal diffusivity was independent of its initial value. In the following, an average value of 8.10^{-7} $m^2.s^{-1}$ was considered as the initial value of the thermal diffusivity.

4.2.2 Influence of the uncertainty of the temperature variations

To estimate the influence of the uncertainty of the temperature variations on the results, the following process was performed:

- A random noise measurement with a standard deviation of ± 0.1 °C was added to each temperature measurement.

- The analytical model was applied considering these noisy temperatures.

This process was repeated 100 times for each sensor couple. The mean value and the standard deviation were calculated for the first heating cycle (Table 1). The results showed that a standard deviation of 0.1 °C of the temperature values has a negligible standard deviation (less than 0.05%) for the thermal diffusivity estimation.

Table 1 : Standard deviation evaluation consideing a 0.1°C error on the temperature measure and errores due to the the variation of the distance (0.001 m) between the temperature sensors from the axis of container. r_1 and r_2 are the distance of the sensors from the axis of the container.

Tr_2	Tr_1	r_2 m	r_1 m	α $(10^{-7}m^2.s^{-1})$ Estimated	α $(10^{-7}m^2.s^{-1})$ Mean	standard deviation %	Error %
T3	T4	0.25	0.15	10.08	10.08	0.05	2
T3	T5	0.25	0	10.24	10.24	0.03	1
T4	T5	0.15	0	10.49	10.49	0.03	2
T6	T5	0.15	0	8.68	8.68	0.04	1
T7	T5	0.25	0	9.21	9.21	0.02	0
T7	T6	0.25	0.15	9.52	9.52	0.04	1

4.2.3 Influence of the distance variations on thermal diffusivity estimation

The main uncertainty of the model is related to the distances of the temperature sensors to the centre of the container. In the laboratory, the relative positions of the temperature sensors inside the container were accurately known, but in the field, the initial position of each temperature sensor may change over time throughout their setting in the soil layer and throughout the length of the structure. To estimate the influence of a distance error, the following process has been carried out:

- Estimation of the thermal diffusivity with nominal values r_1 and r_2.

- Estimation of the thermal diffusivity with the following pairs of radii $(r_1 + \delta r, r_2 + \delta r), (r_1 + \delta r, r_2 - \delta r), (r_1 - \delta r, r_2 + \delta r)$, and $(r_1 - \delta r, r_2 - \delta r)$, where δr is the distance error (10^{-3} m).

The maximum deviation between these 4 estimated thermal diffusivity values and the first one has been considered as the estimated error. The process was applied to each pair of probes (Table 1). The accuracy of the estimation of the thermal diffusivity is less than 2% for any pair of temperature sensors.

It should be noted that an error as high as 10 mm in the position of temperature sensor T5 (r_1 =0) would have a negligible influence on the estimated α (a deviation less than 0.5%). This is

because $I_0(r = 0) = 0$ and the derivative of I_0 at the vicinity of 0 is small. In contrast, an error of 5 mm in the position of temperature sensor T6 (r_2 =0.15 m) led to an error of 6.8%. Consequently, the position of the temperature sensors must be accurately known to use this method. In some cases, (such as for T6), the method could lead to a significant estimation error.

4.3 *Thermal properties estimated with the TFEM*

The thermal diffusivity value α ($m^2.s^{-1}$) for each section between 2 temperature sensors (Tr_2 and Tr_1) is listed in Table 2. The average thermal diffusivity was 9.6×10^{-7} $m^2.s^{-1}$ for the first heating cycle and 9.4×10^{-7} $m^2.s^{-1}$ for the second and third heating cycles. Busby [43] estimates the thermal properties of different types of soil by utilizing a British database of meteorological soil temperature measurements obtained at a depth of 1 m. The range of the thermal diffusivity values ($5\times10^{-7} \leq \alpha \leq 10^{-6}$ $m^2.s^{-1}$) reported by Busby [43] was consistent with the thermal diffusivity values determined in this study for soils with similar characteristics.

Figure 8a shows the difference recorded between the T5 and T6 measurements, and Figure 8b compares the experimental records with the simulation results considering the estimated parameters for the first cycle. The differences are much smaller than 0.02 °C for a maximum temperature increase of 27 °C, which shows a good agreement between the experimental measurements and the analytical model results and validates the applicability of the 1D heat conduction model.

Table 2: Estimated thermal diffusivity α ($m^2.s^{-1}$) of compacted soil using TFEM and thermal conductivity λ ($W.m^{-1}.K^{-1}$) using α and C_v ($J.m^{-3}.K^{-1}$) measured by calorimetry; r_1 and r_2 are the distance of the sensors from the axis of the container.

					1st cycle		2nd and 3rd cycles	
Tr_2	Tr_1	r_1	r_2	C_v	$10^{-7}\alpha$	λ	$10^{-7}\alpha$	λ
		m	m	$J.m^{-3}.K^{-1}$	$m^2.s^{-1}$	$W.m^{-1}.K^{-1}$	$m^2.s^{-1}$	$W.m^{-1}.K^{-1}$
T3	T4	0.25	0.15	2.64×10^6	10.0	2.64	9.9	2.61
T3	T5	0.25	0		10.2	2.69	10.0	2.64
T4	T5	0.15	0		10.4	2.74	10.3	2.71
T6	T5	0.15	0		8.6	2.27	8.4	2.21
T7	T5	0.25	0		9.2	2.43	9.0	2.37
T7	T6	0.25	0.15		9.5	2.5	9.3	2.45

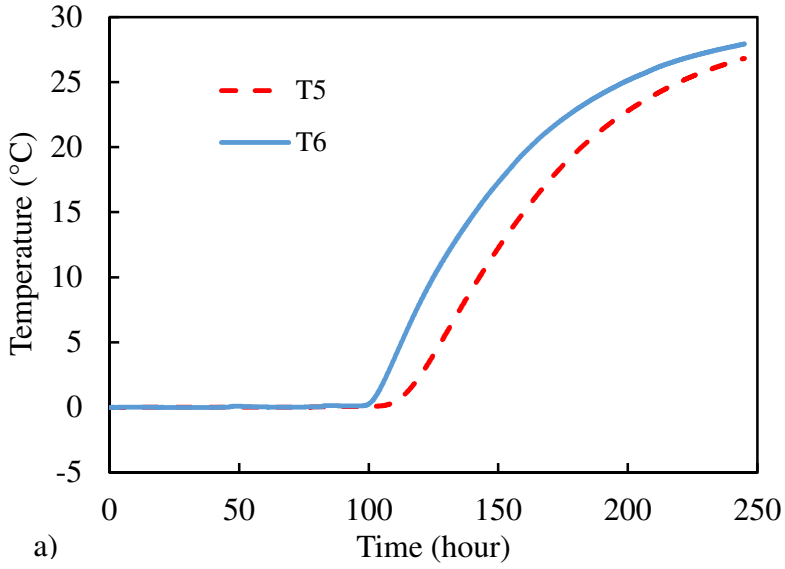

451

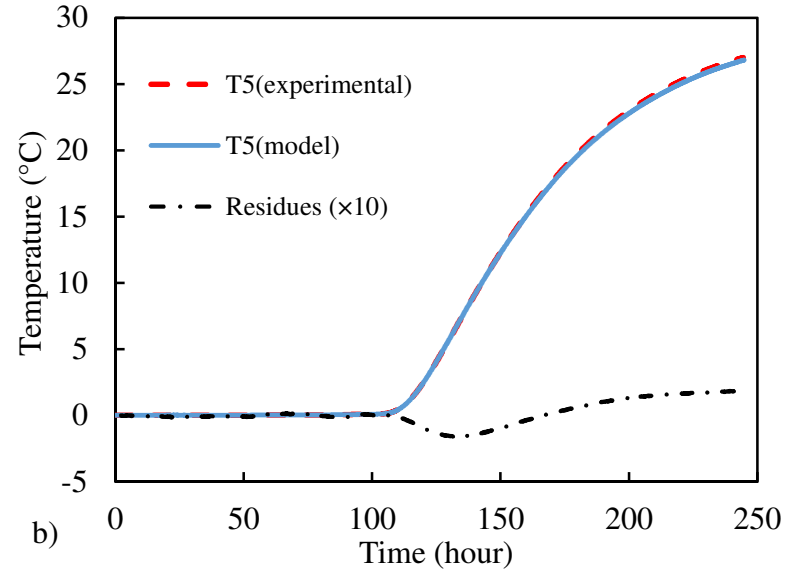

452

453 *Figure 8: a) temperature evolution recorded by T5 and T6 sensors during the first heating cycle*
454 *b) comparison between the experimental and the model values for T5 evolution.*

455 The dry specific heat, C_{dry}, of the dry material as a function of the temperature was measured
456 with a micro-calorimeter. The results are plotted in Figure 9. Then, considering the initial water
457 content (16.3%) of the tested samples, the specific heat, C_p, of the soil was calculated at 20 °C
458 using Eq. (2): C_p=1322 $J.kg^{-1}.K^{-1}$. The volumetric heat capacity evaluated was finally
459 calculated with Eq. (3): $C_v = 2.64\times10^6$ $J.m^{-3}.K^{-1}$.

460

461

462

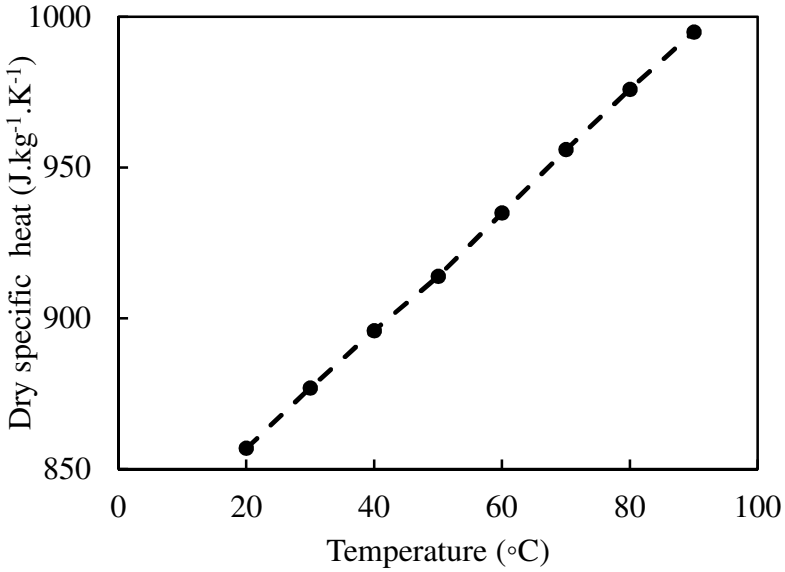

Figure 9: Dry specific heat variation ($\boldsymbol{C_{dry}}$) of the dried soil according to the temperature.

Then, this value of the volumetric heat capacity ($C_v = 2.64\times10^6\ J.m^{-3}.K^{-1}$) was used to calculate the thermal conductivity λ ($W.m^{-1}.K^{-1}$) for each cycle using Eq. (1). Table 2 summarizes the thermal conductivity values calculated for all cycles. The average value for the first cycle was $2.51\pm0.23\ W.m^{-1}.K^{-1}$, and the average value for the second cycle was the same as the third one: $2.47\pm0.25\ W.m^{-1}.K^{-1}$.

4.4 Comparison with the other measurement methods

In this section, the results of the soil thermal conductivity measurements with the needle probe (KD2 pro) and centred hot plate methods are presented. The thermal conductivity of the two samples was measured with the needle-probe device (KD2 pro). The average thermal conductivity of the samples was approximately 2.46 $W.m^{-1}.K^{-1}$ (Table 3).

Two tests were performed with the centred hot plate method (Table 3). The first test lasted 2 days, and the second test lasted 6 days. T_1 denotes the temperature of the heating element controlled by the electrical intensity. During the tests, the temperature of the heating element (T_1) was 24.3 ± 0.76 °C, and the temperature of the aluminium plates (T_{01} and T_{02}) was 14.5 ± 0.5 °C (Table 3). The temperature differences between the heating element and the aluminium plates induced a one-dimensional heat flow from the heating element through the sample towards the aluminium plate. The temperature of the surrounding air in all the tests was kept constant at 23 °C to ensure 1D heat transfer at the centre of the sample. The variation of the thermal conductivity with time for the second test is presented in Figure 10. After one day, the thermal conductivity decreased. This decrease can be explained by considering the water

evaporation under heating, as the sample water content decreased from 16.3% to 14.66% during the second test. Under that condition, the average thermal conductivity of the compacted soil for both tests was 1.97 $\mathrm{W.m^{-1}.K^{-1}}$.

Table 3. Thermal conductivity $\boldsymbol{\lambda}$ ($\boldsymbol{W.m^{-1}.K^{-1}}$) Measurement of the compacted soil with the single needle probe and centred hot plate method.

Method	Single needle probe		Centred hot plate				
Nb.	T (°C)	λ ($\mathrm{W.m^{-1}.K^{-1}}$)	e (m)	T_1	T_{01} (°C)	T_{02}	λ ($\mathrm{W.m^{-1}.K^{-1}}$)
1	23.25	2.42	0.02	23.58	15.30	13.86	1.90
2	20.98	2.50	0.02	25.10	16.51	14.97	2.05
Mean value		2.46					1.97

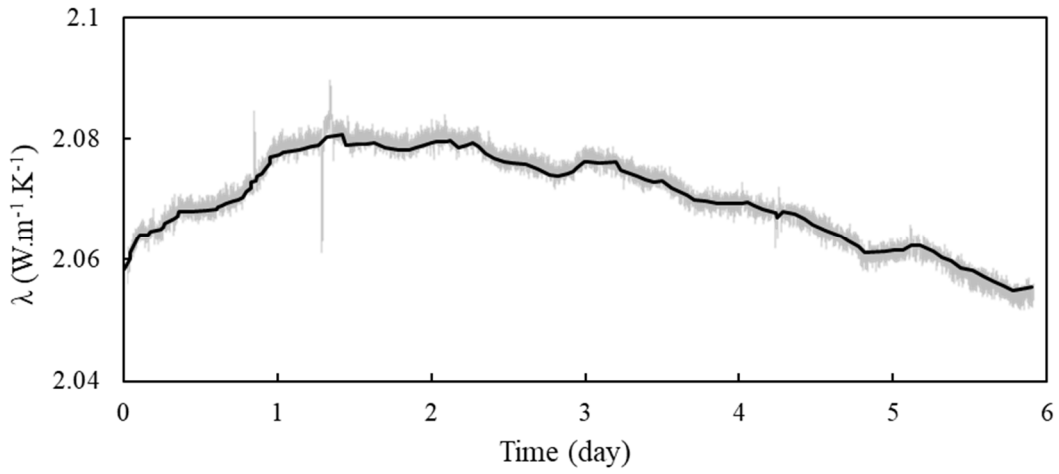

Figure 10 : Variation of the thermal conductivity $\lambda\ (W.m^{-1}.K^{-1})$ during a centred hot plate test on the compacted soil.

The estimated values of the thermal conductivity measured by the TFEM method (2.51 $\mathrm{W.m^{-1}.K^{-1}}$) and by the single-needle probe method (2.46 $\mathrm{W.m^{-1}.K^{-1}}$) are very close (2% deviation). In contrast, the deviation between the values obtained by the TFEM method and the centred hot plate method (1.97 $\mathrm{W.m^{-1}.K^{-1}}$) is quite high (greater than 20%). The thermal contact resistances that were neglected may explain this deviation. The thermal resistance of the soil sample is approximately $R_s = e_s/\lambda_s \approx 0.02/2.5 \approx 8 \times 10^{-3}\ \mathrm{K.m^2.W^{-1}}$ for a sample thickness of $e = 0.02$ m.

Assuming an air layer with a thickness of $e_{air} = 0.025$ mm on each side of the sample, the total thermal contact resistance is $R_{c1} + R_{c2} = 2e_{air}/\lambda_{air} = 2 \times 2.5 \times 10^{-5}/0.025 = 2 \times 10^{-4}$

503 $K.m^2.W^{-1}$. The estimated value with Eq. (23) is $\lambda_s = 1.97\ W.m^{-1}.K^{-1}$. Considering the
504 estimated value of $R_{c1} + R_{c2}$ and using Eq. (22), one obtains: $\lambda_s = 2.45\ W.m^{-1}.K^{-1}$. This
505 value is close to the values obtained with the two transient-state methods. One can conclude
506 that steady-state methods are not suitable for the measurement of thermal conductivities as high
507 as $2.45\ W.m^{-1}.K^{-1}$.

508 5 Conclusions

509 In this study, the thermal properties of an unsaturated compacted soil were investigated. The
510 thermal diffusivity was estimated via a new "temperature/temperature" method based on the
511 estimation of a heat transfer function. One of the main benefits of this method is that it only
512 requires temperature time series measurements at two locations.

513 The thermal conductivity was then estimated based on the estimated values of the thermal
514 diffusivity and the volumetric heat capacity measured by calorimetry and then compared with
515 the values obtained with two other methods (a transient-state method and a steady-state
516 method). The inverse analytical model, generally used to characterize granular powders, was
517 applied to unsaturated compacted soils in this study. The results showed that this simple
518 analytical model has a good agreement (2% deviation) with the experimental results obtained
519 with the transient-state method and the single-needle probe method. In contrast, we have
520 demonstrated that steady-state methods are not suited for this type of material since thermal
521 contact resistances are no longer negligible compared to the sample thermal resistance.

522 In this method, the shape and intensity of the heat flux or the external boundary condition have
523 not been considered, but the hypothesis of transient heat conduction in the radial direction in
524 cylindrical coordinates should be considered. As is generally done, mass transfer is not
525 considered in this model. The main uncertainty of the model is related to the distances of the
526 temperature sensors to the centre of the container, so the distance between two sensors must be
527 accurately measured.

528 The main advantage of this method is its application to in situ measurements. In this analytical
529 model, heat conduction should be applied in the radial direction in cylindrical coordinates. The
530 radial heat flux can be conducted experimentally, from the outer surface of a cylindrical
531 container (as in this study), but under in situ conditions, the radial heat flux can be applied by
532 just considering the cylindrical shape of heat exchanger loops (from the surface of the tubes
533 towards an arbitrary cylindrical surface). In the field, only two temperature sensors should be
534 placed at different distances from the heat exchanger tubes to monitor the temperature

variations; therefore, thermal properties at any time can be estimated. Consequently, this method could enable system efficiency estimation of possible future applications of thermal energy storage in compacted soils such as embankments or other configurations.

6 References

[1] Stojanović, B., & Akander, J. (2010). Build-up and long-term performance test of a full-scale solar-assisted heat pump system for residential heating in Nordic climatic conditions. Applied Thermal Engineering, 30(2), 188-195. https://doi.org/10.1016/j.applthermaleng.2009.08.004

[2] Abedin A.H., & Rosen M.A., A (2011) Critical Review of Thermochemical Energy Storage Systems. Open Renewable Energy Journal, 4, 42-46. https://doi: 10.2174/1876387101004010042

[3] Xu, J., Wang, R. Z., & Li, Y. (2014). A review of available technologies for seasonal thermal energy storage. Solar Energy, 103, 610-638. https://doi.org/10.1016/j.solener.2013.06.006

[4] Li, C., Cleall, P. J., Mao, J., & Muñoz-Criollo, J. J. (2018). Numerical simulation of ground source heat pump systems considering unsaturated soil properties and groundwater flow. Applied Thermal Engineering, 139, 307-316. https://doi.org/10.1016/j.applthermaleng.2018.04.142

[5] Jradi, M., Veje, C., & Jørgensen, B. N. (2017). Performance analysis of a soil-based thermal energy storage system using solar-driven air-source heat pump for Danish buildings sector. Applied Thermal Engineering, 114, 360-373. https://doi.org/10.1016/j.applthermaleng.2016.12.005

[6] Boukelia, A., Eslami, H., Rosin-Paumier, S., & Masrouri, F. (2017). Effect of temperature and initial state on variation of thermal parameters of fine compacted soils. European Journal of Environmental and Civil Engineering, 1-14. https://doi.org/10.1080/19648189.2017.1344144

[7] Romero, E., Gens, A., & Lloret, A. (2001). Temperature effects on the hydraulic behaviour of an unsaturated clay. In Unsaturated Soil Concepts and Their Application in Geotechnical Practice (pp. 311-332). Springer, Dordrecht. https://doi.org/10.1007/978-94-015-9775-3_5.

[8] François, B., Salager, S., El Youssoufi, M. S., Ubals Picanyol, D., Laloui, L., & Saix, C. (2007). Compression tests on a sandy silt at different suction and temperature levels. Computer applications in geotechnical engineering, pp. 1-10.

[9] Uchaipichat, A., & Khalili, N. (2009). Experimental investigation of thermo-hydro-mechanical behaviour of an unsaturated silt. Géotechnique, 59(4), 339-353. https://doi.org/10.1680/geot.2009.59.4.339

[10] Penner, E., Johnston, G. H., & Goodrich, L. E. (1975). Thermal conductivity laboratory studies of some Mackenzie Highway soils. Canadian Geotechnical Journal, 12(3), 271-288. https://doi.org/10.1139/t75-033

570 [11] Abu-Hamdeh, N.H., & Reeder, R.C. (2000). Soil Thermal Conductivity: Effects of Density,
571 Moisture, Salt Concentration, and Organic Matter. Soil Science Society of America Journal,
572 64(4), 1285–1290. https://doi:10.2136/sssaj2000.6441285x
573 [12] Ekwue, E.I., Stone, R.J., & Bhagwat, D. (2006). Thermal Conductivity of Some Compacted
574 Trinidadian Soils as affected by Peat Content. Biosystems Engineering, 94, 461–469.
575 https://doi.org/10.1016/j.biosystemseng.2006.03.002
576 [13] Jahangir, M. H., Ghazvini, M., Pourfayaz, F., & Ahmadi, M. H. (2018). A numerical study into
577 effects of intermittent pump operation on thermal storage in unsaturated porous media. Applied
578 Thermal Engineering, 138, 110-121. https://doi.org/10.1016/j.applthermaleng.2018.04.023
579 [14] Kodikara, J., Rajeev, P., & Rhoden, N. J. (2011). Determination of thermal diffusivity of soil
580 using infrared thermal imaging. Canadian Geotechnical Journal, 48(8), 1295-1302.
581 https://doi.org/10.1139/t11-036
582 [15] Rajeev, P., & Kodikara, J. (2016). Estimating apparent thermal diffusivity of soil using field
583 temperature time series. Geomechanics and Geoengineering, 11(1), 28-46.
584 https://doi.org/10.1080/17486025.2015.1006266
585 [16] Ukrainczyk, N. (2009). Thermal diffusivity estimation using numerical inverse solution for 1D
586 heat conduction. International journal of heat and mass transfer, 52(25-26), 5675-5681.
587 https://doi.org/10.1016/j.ijheatmasstransfer.2009.07.029
588 [17] Abu-Hamdeh, N. H., Khdair, A. I., & Reeder, R. C. (2001). A comparison of two methods used
589 to evaluate thermal conductivity for some soils. International Journal of Heat and Mass
590 Transfer, 44(5), 1073-1078. https://doi.org/10.1016/S0017-9310(00)00144-7
591 [18] Kraemer, D., & Chen, G. (2014). A simple differential steady-state method to measure the
592 thermal conductivity of solid bulk materials with high accuracy. Review of Scientific
593 Instruments, 85(2), 025108. https://doi.org/10.1063/1.4865111
594 [19] Barry-Macaulay, D., Bouazza, A., Singh, R. M., Wang, B., & Ranjith, P. G. (2013). Thermal
595 conductivity of soils and rocks from the Melbourne (Australia) region. Engineering
596 Geology, 164, 131-138. https://doi.org/10.1016/j.enggeo.2013.06.014
597 [20] Dieye, Y., Sambou, V., Faye, M., Thiam, A., Adj, M., & Azilinon, D. (2017). Thermo-
598 mechanical characterization of a building material based on Typha Australis. Journal of
599 Building Engineering, 9, 142-146. https://doi.org/10.1016/j.jobe.2016.12.007
600 [21] Jannot, Y., Felix, V., & Degiovanni, A. (2010). A centered hot plate method for measurement
601 of thermal properties of thin insulating materials. Measurement Science and technology, 21(3),
602 035106 10. https://doi:1088/0957-0233/21/3/035106
603 [22] Jannot, Y., Degiovanni, A., Grigorova-Moutiers, V., & Godefroy, J. (2016). A passive guard
604 for low thermal conductivity measurement of small samples by the hot plate
605 method. Measurement Science and Technology, 28(1), 015008.

606 [23] Bilskie, J. R. (1994). Dual probe methods for determining soil thermal properties: Numerical
607 and laboratory study. PhD thesis, University of Iowa State, Ames, Lowa, United States. 10679.
608 [24] Coquard, R., Baillis, D., & Quenard, D. (2006). Experimental and theoretical study of the hot-
609 wire method applied to low-density thermal insulators. International journal of heat and mass
610 transfer, 49(23-24), 4511-4524. https://doi.org/10.1016/j.ijheatmasstransfer.2006.05.016
611 [25] Asrar, G., & Kanemasu, E. T. (1983). Estimating Thermal Diffusivity Near the Soil Surface
612 Using Laplace Transform: Uniform Initial Conditions 1. Soil Science Society of America
613 Journal, 47(3), 397-401. https://doi:10.2136/sssaj1983.03615995004700030001x
614 [26] Gehlin S., & G. Hellström (2000). Recent Status of In-situ Thermal Response Tests for BTES
615 Applications in Sweden. Proc. Terrastock'2000, August 28th September 1st , Stuttgart, Germany,
616 pp 159-164.
617 [27] Gehlin, S., & Nordell, B. (2003). Determining undisturbed ground temperature for thermal
618 response test. ASHRAE Transactions, 109, (1), pp. 151-156.
619 [28] Beier, R. A. (2018). Use of temperature derivative to analyze thermal response tests on borehole
620 heat exchangers. Applied Thermal Engineering, 134, 298-309.
621 https://doi.org/10.1016/j.applthermaleng.2018.02.004.
622 [29] Adams, W. M., Watts, G., & Mason, G. (1976). Estimation of thermal diffusivity from field
623 observations of temperature as a function of time and depth. American Mineralogist, 61(7-8),
624 560-568.
625 [30] Horton, R., Wierenga, P. J., & Nielsen, D. R. (1983). Evaluation of Methods for Determining
626 the Apparent Thermal Diffusivity of Soil Near the Surface 1. Soil Science Society of America
627 Journal, 47(1), 25-32.
628 [31] Gao, Z., Wang, L., & Horton, R. (2009). Comparison of six algorithms to determine the soil
629 thermal diffusivity at a site in the Loess Plateau of China. Hydrology and Earth System Sciences
630 Discussions, 6, 2247.
631 [32] Jannot, Y., & Degiovanni, A. (2013). Thermal properties measurement of dry bulk materials
632 with a cylindrical three layers device. Review of Scientific Instruments, 84(9), 094901.
633 https://doi.org/10.1063/1.4821083,
634 [33] Boukelia, A., 2016. Physical and numerical modeling of energy geostructures. PhD thesis,
635 University of lorraine, Nancy, France, 187 pp. https://doi.org/10.1139/cgj-2018-0583,
636 [34] AFNOR (1993). NF P94-051: Determination of Atterberg's limits. Liquid limit test using
637 cassagrande apparatus. Plastic limit test on rolled thread] (p. 15). Association Française de
638 Normalisation, Paris, France.
639 [35] AFNOR (1999b). NF P 94-093: Soils: Investigation and testing. Determination of the
640 compaction characteristics of a soil. Standard Proctor test. Modified Proctor test (p. 18).
641 Association Française de Normalisation, Paris, France.

[36] ASTM Standard D2487 (2000). Standard Practice for Classification of Soils for Engineering Purposes (Unified Soil Classification System), ASTM International, West Conshohocken, PA.

[37] GTR (2000). Réalisation des remblais et des couches de forme. Laboratoire Central des Ponts et Chaussées, Paris, p. 102.

[38] Bristow, K. L. (1998). Measurement of thermal properties and water content of unsaturated sandy soil using dual-probe heat-pulse probes. Agricultural and forest meteorology, 89(2), 75-84. https://doi.org/10.1016/S0168-1923(97)00065-8

[39] Smits, K. M., Sakaki, T., Limsuwat, A., & Illangasekare, T. H. (2010). Thermal conductivity of sands under varying moisture and porosity in drainage–wetting cycles. Vadose Zone Journal, 9(1), 172-180. https://doi:10.2136/vzj2009.0095

[40] Devices, D. (2016). KD2 pro thermal properties analyzer operator's manual. Pullman, WA.

[41] Jannot, Y., Moyne, C. (2018). Thermal properties measurements of materials. ISTE Wiley, edition, p. 299.

[42] De Hoog, F. R., Knight, J. H., & Stokes, A. N. (1982). An improved method for numerical inversion of Laplace transforms. SIAM Journal on Scientific and Statistical Computing, 3(3), 357-366. https://doi.org/10.1137/0903022

[43] Busby, J. (2015). Determination of thermal properties for horizontal ground collector loops. Proc. World Geothermal Congress 2015, 19-25 April, Melbourne, Australia http://wgc2015.com.au/

Nomenclature

List of abbreviations

TFEM	Transfer function estimation method
THM	Thermo-hydro-mechanical
LL	Liquid limit
PL	Plastic limit
PI	Plasticity index
DSC	Micro differential scanning calorimeter
$\otimes$	The convolution operator

List of symbols

C_p	Specific heat $(J.kg^{-1}.K^{-1})$
C_{dry}	Specific heat of dry material $(J.kg^{-1}.K^{-1})$
C_{water}	Specific heat of pure water $(J.kg^{-1}.K^{-1})$
C_v	Volumetric heat capacity $(J.m^{-3}.K^{-1})$
r	Radius (m)
R	Radius of container (m)
p	Laplace parameter (s^{-1})
F	Transfer function (s^{-1})
e	Thickness (m)
R_s	Thermal resistance $K.m^2.W^{-1}$
R_{c1}	Thermal contact resistances of sample and heating element $K.m^2.W^{-1}$
R_{c2}	Thermal contact resistances of sample and aluminum plate $K.m^2.W^{-1}$
H	Laplace transform of the transform function
m_0	Ambient temperature for heating (K)
m_1	Ambient temperature for cooling (K)
m_2	Rate of background temperature drift $(K.s^{-1})$
m_3	Slope of a line relating temperature rise to the logarithm of temperature (K)
Q	Applied heat input rate per unit length $(W.m^{-1})$
t	Time (s)
T	Temperature (K)
T_h	Temperature during heating phase (K)
T_c	Temperature during cooling phase (K)
T_0	Temperature of heating element (K)

T_{01}	Temperature of aluminum plate (K)
T_{02}	Temperature of aluminum plate (K)

List of Greek letters

λ	Thermal conductivity ($W.m^{-1}.K^{-1}$)
α	Thermal diffusivity ($m^2.s^{-1}$)
w	Water content (%)
ρ	Density ($Mg.m^{-3}$)
$\theta(p)$	Laplace transform of the temperature (K. s)
φ	Heat flux (W)

List of subscripts

in	Inflow
i	Initial
out	Outflow
h	Heating
air	Air
s	Soil
opt	Optimum
d	Dry
ref	Reference material

674

675